Research Article | Vol. 11, No. 12 / 1 December 2020 / Biomedical Optics Express 7062
Biomedical Optics EXPRESS

Highly sensitive detection of cytochrome c in the NSCLC serum using a hydrophobic paper based–gold nanourchin substrate

YUE SUN,[1,2] SHENGJIE GE,[1,2] JIN XUE,[3] XINYU ZHOU,[1,2] WENBO LU,[4] GUANG LI,[5] AND XIAOWEI CAO[1,2,6,*]

[1]Institute of Translational Medicine, Medical College, Yangzhou University, Yangzhou 225001, China
[2]Jiangsu Key Laboratory of Experimental and Translational Non-coding RNA Research, Medical College, Yangzhou University, Yangzhou 225001, China
[3]Guangling College, Yangzhou University, Yangzhou 225001, China
[4]Shanxi Normal University, College of Chemistry and Material Science, Linfen 041004, China
[5]Department of Otorhinolaryngology, Affiliated Hospital of Yangzhou University, Yangzhou 225001, China
[6]Jiangsu Key Laboratory of Zoonosis, Yangzhou University, Yangzhou 225009, China
*cxw19861121@163.com

Abstract: Cytochrome c (Cyt c) is a biomarker of early apoptosis that plays a critical role in the diagnosis and therapy of non-small cell lung cancer (NSCLC). In this work, we proposed a novel surface-enhanced Raman scattering (SERS)-based biosensor to implement the ultrasensitive detection of Cyt c in the serum of NSCLC patients. The SERS-supporting substrates based on hydrophobic filter paper were composed of gold nanourchins (GNUs) surface-functionalized with the Cyt c aptamer and the cyanine 5-labeled complementary DNA. In the existence of Cyt c, it could specifically bind to its aptamer, which leads to the detachment of complementary strands modified with Cy5 and the great weakness of SERS signal. The finite-difference time domain (FDTD) simulation showed that the excellent SERS performance of GNUs aggregation was strongly dependent on a large number of "hot spots" at the tips and between the nanogaps of aggregated GNUs. Alkyl ketene dimer (AKD) was used to make the filter paper modify its property from hydrophilic to hydrophobic, which consequently increased the density of GNUs and extended the retention time of the analyte. SERS biosensors based on hydrophobic paper exhibited prominent reproducibility and selectivity. The detection limit of Cyt c in PBS was 1.148 pg/mL, while the detection limit in human serum was 1.79 pg/mL. Moreover, the analysis of the serum samples of healthy subjects and NSCLC patients confirmed the feasibility of its clinical application. The results were consistent with enzyme-linked immunosorbent assay results. This method can be a powerful strategy for quantitative detection of extracellular Cyt c, and it is expected that the SERS-based biosensors could be applied in the practical clinical diagnoses of NSCLC.

1. Introduction

Lung cancer has become one of the most common malignancies worldwide [1]. The majority of lung cancer patients are diagnosed with non-small cell lung cancer (NSCLC), including lung adenocarcinoma, lung squamous carcinoma, and large cell lung cancer [2,3]. Lung cancer is the most commonly diagnosed cancer in both sexes, with a total of 11.6% of the cases. Lung cancer accounts for 18.4% of the cancer deaths, and its aggressiveness is the main reason for the high mortality rate [4]. In fact, most NSCLC is usually diagnosed at the late stage of inoperable stage, although early detection of NSCLC significantly improves survival rate. Therefore, early diagnosis is of great significance to improve the prognosis and prolong the survival time of lung cancer patients. Recent studies have shown that serum cytochrome c is a potential marker for

#408649 https://doi.org/10.1364/BOE.408649
Journal © 2020 Received 27 Aug 2020; revised 21 Oct 2020; accepted 22 Oct 2020; published 10 Nov 2020

Biomedical Optics EXPRESS

diagnosing NSCLC [5]. Cytochrome c (Cyt c), a water-soluble heme protein, plays an important role in initiation of apoptosis [6,7]. NSCLC patients exhibit more than three times lower serum Cyt c level at the time of diagnosis compared to healthy controls, which indicated that apoptosis is inhibited, enhancing cancer cell proliferation, invasion and migration [8]. In a word, Cyt c can be regarded as an important indicator of NSCLC. However, the early diagnosis of NSCLC still faces many challenges. At present, several conventional methods involving magnetic resonance imaging, sputum cytology examination and histology of bronchoscopy are usually not practical, and are expensive for most early NSCLC detection [9]. These shortcomings prevent tumor diagnosis and differentiation from further clinical application. Moreover, the concentration of Cyt c in human serum is too low to be conducive to detection [5]. Hence it is necessary to develop a novel and simple method for the detection of Cyt c in the early screening of NSCLC.

Surface-enhanced Raman spectroscopy (SERS) is an vibrational spectroscopic technique, which has been proven to be one of the most sensitive analytical methods for the detection of disease biomarkers including proteins, peptides, and nucleic acids [10–13]. In comparison with the traditional analytical method, SERS possesses a good deal of significant superiorities. Above all, SERS demonstrates excellent characteristics with high sensitivity, a unique fingerprint, narrow spectral band, and non-destructive data acquisition [14–16]. Secondly, it is able to facilitate the molecular-level identification of samples [17]. Thirdly, the sample preparation and operation are very easy and nondestructive, which is suitable for the detection of a wide variety of matrices [18,19]. SERS signals can be enhanced by 5 to 6 orders of magnitude in the presence of a reporter molecule near the plasmonic nanoparticles, with values up to 10^{10} at the "hot spots" [20,21]. These "hot spots" are usually found near the edges and vertices of sharp features on isolated nanoparticles or at the junction between electromagnetically coupled nanoparticles [22–24]. As a result, SERS-based sensing, as an ultrasensitive sensing strategy, has attracted wide attention, which has been rapidly developed for biosensing. Aptamer is a piece of single-stranded DNA or RNA sequence isolated through in vitro selection (SELEX, systematic evolution of ligands by exponential enrichment), which is a new class of targeting moieties [25–27]. Due to their capability of folding into secondary and tertiary structures, aptamers are prone to synthesis and manipulation with different functional groups, which enables targeting a wide range of biomarkers with high affinity [28,29]. They offer advantages of low immunogenicity, long-term stability both in solution and a dry powder, high sensitivity, and good specificity [30–32]. Combining the high selectivity of the aptamer reaction with the highly sensitive SERS is a major innovation in nanoplasma, which has achieved good results in recent years. For example, Bhamidipati et al. reported a SERS-based substrate comprising gold nanostars and epithelial cell adhesion molecule (EpCAM) aptamers for the quantification of the cancer biomarker EpCAM protein, both soluble and cell membrane-embedded [28]. Wang et al. constructed a novel SERS biosensing platform consisting of the aptamer sequences of DNA hydrogel and AuNPs SERS probes for the sensitive detection of α-fetoprotein (AFP) in human serum, a tumor marker of liver cancer [33]. Li et al. developed an ultrasensitive biosensor to detect protein tyrosine kinase-7 (PTK7) in blood samples, an important tumor biomarker on the cell surface, by aptamer conformation-cooperated enzyme-assisted surface-enhanced Raman scattering (SERS) (ACCESS) technology [34]. The use of aptamers provided the highly specific recognition for SERS tags, which can achieve the quantitative and specific detection of a variety of biomarkers and accurate diagnosis of diseases.

In order to detect bioactive molecules at trace level, SERS signals should be further enhanced through preparing optimized nanostructures with high density of "hot spots" [35]. The enhanced amplification of the SERS signal arises from the localized surface plasmon resonance (LSPR) of the metal-based nanostructure [36–38]. With the LSPR excited, an intense electromagnetic field (EM), which is called "hot spot", is generated in the proximity of the metal nanoparticles, amplifying the SERS signal [39,40]. The properties of nanoparticles, such as size, shape and aggregation, powerfully influence the resonance of LSPR [23]. As is known to all, the presence

Biomedical Optics EXPRESS

of numerous "hot spots" results in the achievement of the strong EM enhancement at interparticle gaps, tips, and protrusions [41,42]. According to the basic principle, nanomaterials with special protrusions and multiple branch angles, which have higher SERS enhancement or contain a higher density of "hot spots", have attracted great attention for SERS development. In comparison with other nanomaterials, gold nanourchins (GNUs), which are composed of many sharp protrusions and tips, have been proven to produce strong local electromagnetic field enhancement up to about 10^9 in order of magnitudes [43]. Optically excited plasmonic hot spots are located at the multi-sharp tips of GNUs, enhancing the electromagnetic field around the nanoparticles [44]. GNUs have good biocompatibility, low preparation cost, mild synthesis conditions and simple reaction process. As a result, GNUs are a potential candidate for the construction of SERS substrates to detect biomolecules. In contrast with isolated nanoparticles, the aggregates of nanoparticles have a more significant electromagnetic field coupling, which tends to increase with the decrease of nanoparticle gap [45,46]. GNUs were assembled into substrates to achieve hot spots with high density and strong SERS signal enhancement effect.

Speaking generally, to use SERS technology in routine studies for analysis, the SERS substrates should be cheap, stable, easily producible and ecologically friendly [47]. For these reasons, researchers have been absorbed in paper-based SERS substrates as an excellent replacement for conventional SERS substrates recently [47–49]. However, the sensitivity and reproducibility of the sensors are reduced on account of the inherent nature of paper substrates for SERS sensors, such as high porosity, hygroscopic nature, and hydrophilic surface properties, which limit their use [48]. In this paper, we proposed a filter paper functionalized with alkyl ketene dimer (AKD) for hydrophilic-to-hydrophobic surface property modification. The paper was treated with AKD to make the hydroxyl groups of the cellulose fibers in the paper converted into hydrophobic alkyl groups. The homogeneity and reproducibility of the substrate could be improved by preventing the rapid absorption of analytes and nanoparticles into the AKD-treated paper [47].

In this study, the SERS-based biosensor was developed for ultrasensitive detection of Cyt c in clinical serum by using the GNUs immune substrate based on hydrophobic filter paper. Compared with conventional SERS substrates, the hydrophobic paper-based SERS substrates had several advantages of low cost, easy to be functionalized and environmentally friendly [50]. The GNUs substrates with high SERS activity were prepared and modified with Cyt c aptamer and Raman reporter Cy5-labeled complementary DNA as capturing substrates. In order to analyse the SERS homogeneity and stability of the substrates, detailed characterization of the substrates was carried out using scanning electron microscopy (SEM), SERS maps, and SERS spectra. The feasibility of the proposed approach was evaluated through the change of SERS signal during Cyt c detection. The experimental conditions were optimized for the fabrication of the SERS biosensor platform, including the concentration of Cyt c aptamer, the concentration of Cy5-labeled complementary DNA, hybridization time, incubation time of aptamer bonding to Cyt c, and pH values. The selectivity, sensitivity and reproducibility were further evaluated to confirm the performance of the SERS biosensor. The accuracy of the SERS method for testing Cyt c was validated using the ELISA method for comparison. It can be believed that this approach was not only used in the quantitative determination of Cyt c, but also expected to be a new strategy for early diagnosis of NSCLC.

2. Materials and methods

2.1. Materials

Chloroauric acid ($HAuCl_4 \cdot 4H_2O$, analytical grade), L-dopa (3,4-dihydroxyphenylalanine, analytical grade), alkyl ketene dimer (AKD) and filter paper were purchased from Younuo Chemicals Inc. (Yangzhou, China). Glucose (Glu), immunization globulin G (lgG), human serum albumin (HSA), bovine serum albumin (BSA), ascorbic acid (AA) and Cyt c were obtained from Noah Chemical Inc. (Yangzhou, China). Human Cyt c ELISA kit was

Biomedical Optics EXPRESS

purchased from Sangon Biotech Inc. (Shanghai, China). The thiolated aptamer of Cyt c and its complementary strand DNA were purchased from corporation of Minneapolis and were used according to the instructions of manufacturer. Cyt c aptamer sequence: 5'-SH-AGTGTGAAATATCTAAACTAAATGTGGAGGGTGGGACGGGAAGAAGTTTATTTTTCACACT-3'; complementary chain sequence: 5'-ATATTTCACACT-Cy5-3'. Ultrapure water from a Millipore water purification system (18.2 MΩ) was used in the process.

2.2. Synthesis of gold nanourchins

To synthesize gold nanourchins, 2 mL of $HAuCl_4$ solution (10 mM) was injected into 6 mL of ultrapure water. After stirring at 600 rpm for 5 min, 2 mL of L-dopa (10 mM) was added, which made the color of the solution changed from pale yellow to coral. Then, it was allowed to react with agitation for 20 min. Finally, the mixture were centrifuged at 5000 rpm for 5 min and resuspended in 10 mL ultrapure H_2O. All reactions were carried out at room temperature.

2.3. Construction of the SERS substrates

At first, the filter papers were cut to a size of 80 mm by 50 mm, and then soaked in 0.1% AKD dispersion for 2 min to increase its hydrophobicity. After AKD treatment, the filter papers were rinsed with ultrapure water to eliminate the remaining AKD, and then placed in an oven at 100 °C for 10 min to obtain the hydrophobic paper (h-paper). For the fabrication of the GNUs substrates on the h-paper, the h-paper was immersed in the GNUs solution for 12 h. The gold content of GNUs solution was 0.39 mg/mL. They were washed three times with ultrapure water and dried at room temperature. The following step was the surface functionalization of the substrates. The Cyt c aptamer and Cyt c aptamer complementary strand, as DNA, was placed in a water bath at a temperature above melting temperature (T_m) for 5 min to activate the DNA. The T_m was calculated by corporation of Minneapolis. Next, the GNUs substrates were incubated with 50 μL of 1 μM Cyt c aptamer solution (coating) for 80 min. They were washed three times with ultrapure water to remove the excess aptamer. Then the Cyt c aptamer modified GNUs substrates were incubated with 50 μL of 500 nM Cyt c aptamer complementary strand solution (coating). After incubation at 37 °C for 50 min, the hybridization was completed and then the SERS substrates were washed twice with PBS to remove excess unreacted reagent [51]. Finally, the above functionalized substrates were dried at room temperature to obtain the final substrate for SERS measurement.

2.4. Serum sample collection and processing

Serum samples from healthy people and NSCLC patients (both from Subei People Hospital of Jiangsu Province, China) were stored at 4 °C prior to use. All the written consent and ethics permission were acquired. The detailed information of study population was summarized in Table 1. Each blood sample was approximately 5 mL in volume and was extracted intravenously from volunteers before breakfast to avoid the interference of food. Then, the blood sample was deposited at 4 °C for 4 h and was centrifuged at 3000 rpm for 10 min in order to remove the blood cells, fibrinogen, and platelets. The separated supernatants were stored at -80 °C for subsequent experiments.

2.5. Procedure for detecting Cyt c

A 10 μL of target Cyt c solution with different concentrations was added to the above SERS substrate and incubated at 37 °C for 120 min at a humid chamber. The obtained substrate was thoroughly washed by PBS, and was subjected to spectral acquisition.

Biomedical Optics EXPRESS

Table 1. Demographics of study population.

Sample	Healthy subjects	NSCLC
Mean age (years)	45	48
Gender		
Male	16	15
Female	14	15
Sample number	30	30

2.6. Characterization

The UV-visible absorption spectra were obtained by a Hitachi U-3000 UV-visible spectrophotometer. Scanning electron microscope (SEM) images were recorded on an S-4800 II field-emission scanning electron microscope at 3.0 KV. The shape of the nanostructures was characterized by a Tecnai 12 transmission electron microscope at 60 KV (Philips). High-resolution TEM images (HRTEM) and selected area electron diffraction (SAED) images were captured with a Tecnai G2 F30 S-Twin TEM at 200 KV (FEI). SERS spectroscopy measurements were performed by Renishaw Invia microRaman at room temperature by a 785 nm excitation laser. The laser was focused onto the sample surface by a 50× long working distance objective. The extinction power and the acquisition time were 5 mW and 10 s in all measurements, respectively.

3. Results and discussion

3.1. Principle of the Cyt c detection mechanism

Figure 1 is the schematic representation of the SERS-based biosensor for Cyt c detection. First, filter paper was treated with alkyl ketene dimer (AKD) solution to allow an esterification reaction of AKD with the hydroxyl groups of the cellulose fibers in the filter paper. AKD treatment converted the hydroxyl groups of the cellulose fibers in the paper into hydrophobic alkyl groups, which changed the filter paper from hydrophilic to hydrophobic [47,52]. Then, GNUs were assembled to the surface of the AKD functionalized substrates. The next step in the substrate preparation was the in situ functionalization of the GNUs substrate. Due to the sulfhydryl groups at the 5' terminus of the chain, Cyt c aptamers were efficiently chemisorbed on the surface of GNUs through strong gold sulfur bonds. Then the aptamer was connected with a complementary DNA labeled by Cy5 at the 3' terminus by hybridization effect. Finally, the biosensors were successfully prepared. In the presence of Cyt c, the biosensors were triggered because of the specific binding of Cyt c to its aptamer, leading to the detachment of the complementary chains modified with Cy5. The SERS signal of Cy5 weakened gradually with the increase of the distance between the complementary chain and GNUs. Based on this principle, Cyt c in clinical serum could be detected and quantified by the change of SERS signals.

3.2. Characterization of GNUs

The morphology and structure of the as-prepared GNUs were characterized by SEM and TEM. Figure 2(A) showed these GNUs were uniform in both size and morphology. To obtain more detailed observations of the GNUs, a high-magnification SEM image was taken. As shown in Fig. 2(B), the surfaces of the GNUs were closely covered by many thorn-like tips extending radially from a center with few nanometers in thickness and several tens of nanometers in length. The GNUs with the average size were about 300 nm. The typical TEM image of the GNUs in Fig. 2(C) showed that the GNUs were almost the same in morphology and no other shapes were found. The crystal structure and growth surface of the GNUs were observed from HRTEM and SAED images. It can be seen from the HRTEM image in Fig. 2(D) that the GNUs grew

Biomedical Optics EXPRESS

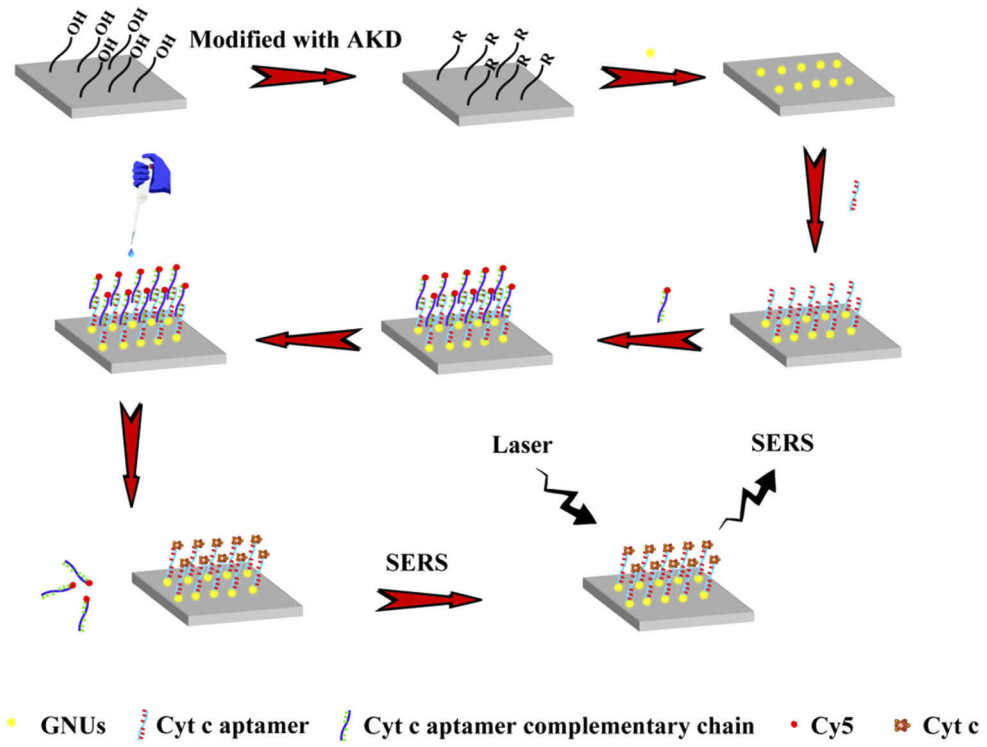

Fig. 1. Schematic illustration of Cyt c detection mechanism with GNUs biosensors based on SERS.

preferentially on (111) planes due to the lattice spacing of the tips of 0.230 nm. The morphology of the GNUs was further observed by SAED image. Several bright apertures in Fig. 2(E) corresponded to (111), (200), (220), (311) crystalline facet respectively, indicating that the GNUs were well-crystallized pure gold nanoparticles. From the representative UV-visible absorption spectrum of the GNUs in Fig. 2(F), the surface plasmon (SP) resonance band of gold is not obvious because of the strong background from the visible light absorption of L-dopa molecules [53]. When $HAuCl_4$ was mixed with L-dopa aqueous solution under stirring at room temperature (as shown in the experiment section), the color of the solution changed from pale yellow to coral within 20 min, which indicated the formation of the GNUs. During the preparation of GNUs, the L-dopa molecules have three important functions. At first, they play the role of a reducing agent to make the Au ions reduced to the Au atoms. Secondly, they serve as capping agents, stabilizing the Au atoms and allowing them to bond together into aggregates. Thirdly, the L-dopa molecules can make Au ions preferentially adsorbed on the tips of the rough surface, which results in a protuberant growth on the surface of the above aggregates with higher curvature. Finally, GNUs can be successfully synthesized in high yields through one-step reduction synthesis [54].

3.3. *Finite-difference time domain (FDTD) simulation*

To understand the interactions of SERS enhancement effect with the GNUs structures, the finite difference time domain (FDTD) method was applied for calculations. It can be seen from the TEM images of GNUs in Figs. 3(A) and 3(B) that the GNUs had an average size of 300 nm, thorn-like tips thickness of 10 nm and thorn-like tips length of 40 nm. The spacing between two GNUs was about 0.5 nm. Figure 3(C) presented the calculated electromagnetic field distribution of the individual GNU at the 785 nm incident laser wavelengths. It was obvious that the "hot

Biomedical Optics EXPRESS

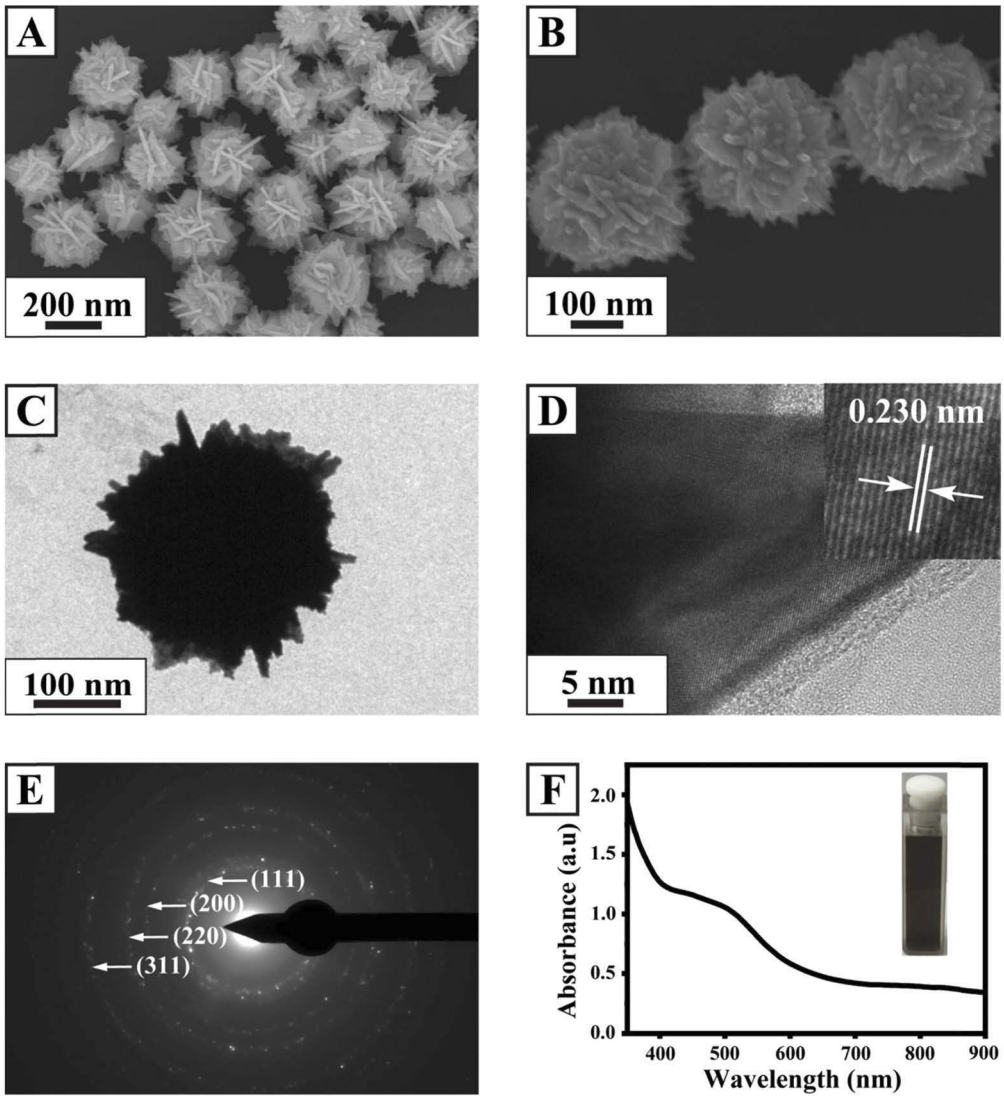

Fig. 2. Typical SEM (A, B) and TEM (C) images of the GNUs. (D) The HRTEM image of the GNUs. (E) The SAED pattern of the GNUs. (F) The representative UV-visible absorption spectrum of the GNUs. The insert shows the solution of the GNUs.

Biomedical Optics EXPRESS

spots" or maxima in |E| were located in the sharp tips and the nanogaps between adjacent tips of the GNUs, showing a strong electromagnetic field enhancement effect [55]. In addition, the interparticles electromagnetic field enhancement effect between GNUs was also investigated in Fig. 3(D). It can be found from the electromagnetic field distribution that additional "hot spots" can be created in the nanogap junction of GNUs dimer via the interparticles assembly, which is greatly beneficial to the improvement of the uniformity and reproducibility of SERS signals [56].

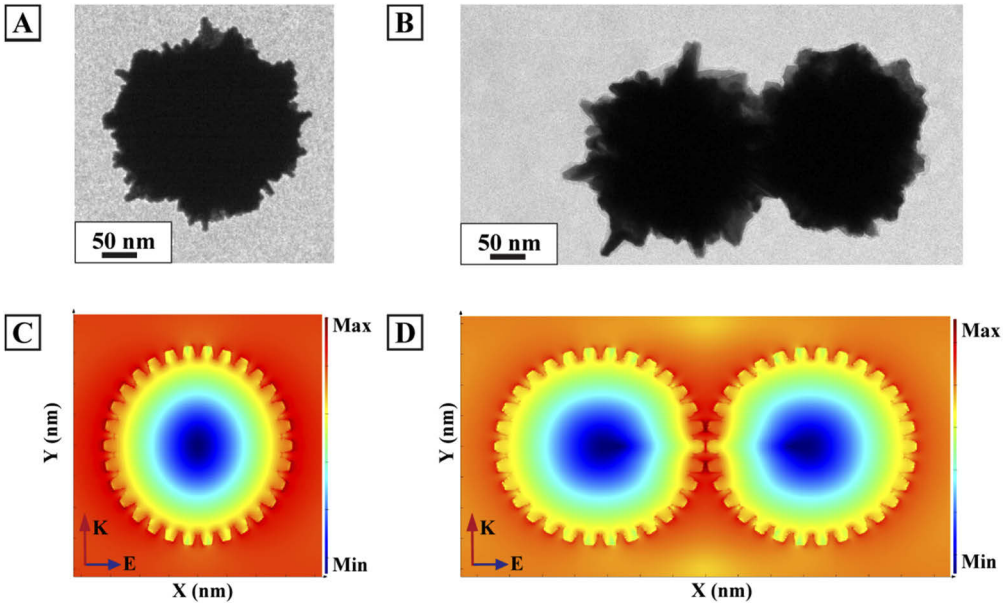

Fig. 3. TEM images of (A) a single GNU, (B) GNUs dimer. The corresponding simulated electric field distribution images of (C) a single GNU, (D) GNUs dimer.

3.4. *Characterization of GNUs substrates*

GNUs substrate was prepared by simple AKD-hydrophobic surface-assembly method. The paper was modified with AKD to generate a hydrophobic top layer, holding back the mainly aqueous sample from spreading on the paper and increasing retention time of analytes. GNUs-modified h-paper substrate was prepared by the sedimentary self-fixing method, making the GNUs deposited on the surface of h-paper. Figures 4(A) and 4(B) displayed the SEM images of GNUs-modified paper substrate and GNUs-modified h-paper substrate, respectively. In comparison with the uneven distribution on the surface of GNUs-modified paper substrate, GNUs-modified h-paper substrate was uniformly distributed on the surface of the h-paper with slight aggregation. The uniformity and enhancement effect of SERS signals were evaluated via a SERS mapping experiment performed by the Renishaw Raman microspectroscopy system. Figures 4(C) and 4(D) presented the SERS mapping images recorded on the GNUs-modified paper substrate and GNUs-modified h-paper substrate. The two prepared substrates were labeled with NBA (5×10^{-6} M), therefore the characteristic peak of NBA at 592 cm^{-1} was used as the mapping signal. The scan area was 40×50 mm^2, the step size was 2 mm, the laser power was 5 mW, and the acquisition time at each point was 10 s. The color of SERS mapping was used to display the intensity of the 592 cm^{-1} at each point according to a color scheme ranging from blue (lowest intensity) through green, yellow, orange, and red (highest intensity). Uneven color distribution in Fig. 4(C) showed that the SERS enhancement effect on the GNUs-modified paper substrate was properly inhomogenous. Instead, the color distribution was uniform in Fig. 4(D),

Biomedical Optics EXPRESS

which indicated that GNUs-modified h-paper substrate had a great homogeneity. Then, the strongest point and the weakest point on two substrates were selected to measure their SERS spectra. In Fig. 4(E), the deviation of the signal intensities at 592 cm^{-1} at the two points on the GNUs-modified paper substrate was 40.19%. While, from Fig. 4(F), the deviation of the signal intensities at 592 cm^{-1} at the two points on the GNUs-modified h-paper substrate was 9.38%, which further supported the good homogeneity of the GNUs-modified h-paper substrate. Therefore, GNUs-modified h-paper substrate was used for the follow-up experiment. In addition to testing the uniformity of the GNUs-modified h-paper substrate, the SERS stability of the NBA-labeled GNUs substrate was also evaluated. As shown in Fig. 4(G), the average SERS spectra of the NBA-labeled GNUs substrate were obtained after GNUs substrates were stored for 0 day, 5 days, 10 days, 15 days at room temperature. Due to no significant changes in the SERS spectral peak and shape, the SERS enhancement effect of the GNUs substrates had excellent stability. In Fig. 4(H), after 15 days, compared with the freshly prepared substrates, the SERS enhancement effect was reduced by only 5.45%, which further proved the SERS stability of the GNUs-modified h-paper substrate.

3.5. Investigation of the feasibility

In the paper, we chose Cyt c, a water-soluble heme protein which was identified as a biomarker of mitochondrial apoptotic pathway, as a model disease target for clinical diagnosis of NSCLC. Principle of this aptamer-based biosensing process for Cyt c was shown in Fig. 1. In brief, the GNUs on h-paper substrate were modified with Cyt c aptamer through strong gold sulfur bonds with thiol labeled at the 5' terminus. Then the aptamer was connected with a complementary DNA labeled by Cy5 at the 3' terminus by hybridization effect. In the presence of Cyt c which can be identified by the aptamer, the complementary DNA will be replaced from the aptamer and can be washed away, making SERS signal significantly decreased.

Cy5 was used as Raman reporter to investigate the feasibility of proposed SERS-active substrate for Cyt c detection. Figure 5(A) showed SERS spectra of the GNUs substrate, the GNUs substrate with Cyt c aptamer modification, the GNUs substrate with aptamer and Cy5-labeled complementary DNA, the SERS biosensor in the presence of Cyt c. And Fig. 5(B) was the corresponding intensities bar graphs of characteristic peaks of Cy5 at 1360 cm^{-1}. No SERS signal was detected when there was no aptamer labeled on the surface of the GNUs substrate (curve a), indicating that the SERS signal of the GNUs substrate had no effect on the subsequent detection. When the Cyt c aptamer was modified on the surface of the GNUs substrate (curve b), still no SERS signals were observed because of the absence of Raman reporter molecule near the substrate. From curve c, strong SERS signals were obtained after a Cy5-labeled complementary DNA was added on the surface of the GNUs substrate modified with Cyt c aptamer, especially at 1120, 1230, 1360, 1465 and 1600 cm^{-1}, which correspond to $\upsilon(\text{C-H})_{\text{ip-bend}}$, $\upsilon(\text{C-N})_{\text{stretch}}$, $\upsilon(\text{C=V})_{\text{ring}}$, $\upsilon(\text{C=C})_{\text{ring-stretch}}$ and $\upsilon(\text{C=N})_{\text{stretch}}$ modes of Cy5 and match well with the literature values [57]. The appearance of characteristic peaks of Cy5 reflected the successful modification of Cyt c aptamer with sulfhydryl on the surface of the GNUs substrate by strong gold sulfur bonds from one aspect. Then the Cy5-labeled complementary DNA was hybridized with the aptamer, generating the strong SERS signal due to small distance between Cy5 and GNUs. It was proved that the complementary DNA was effectively decorated on the SERS substrate. The SERS signal for the SERS substrate significantly decreased after Cyt c was added, confirming that after Cyt c binding to aptamer, Cy5-labeled complementary DNA was separated from the surface of the GNUs substrate and washed away (curve d). These results demonstrate the feasibility of using the intensities of characteristic peaks of Cy5 at 1360 cm^{-1} as the quantitative standard for Cyt c detection.

Biomedical Optics EXPRESS

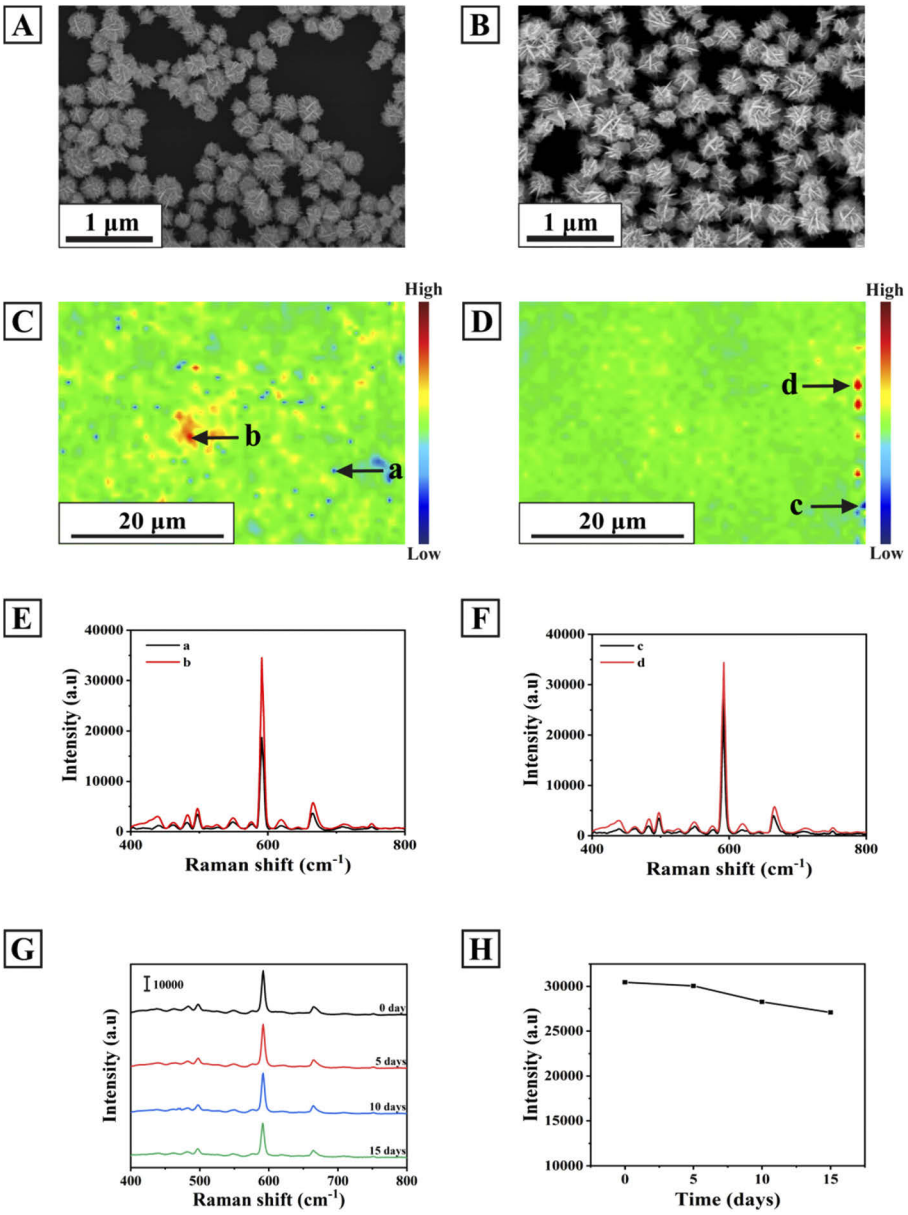

Fig. 4. SEM images of (A) the GNUs-modified paper substrate and (B) the GNUs-modified h-paper substrate. SERS mapping of NBA (5×10^{-6} M) measured at 592 cm^{-1} using (C) the GNUs-modified paper substrate and (D) the GNUs-modified h-paper substrate. (E) The SERS spectra at the strongest point (Fig. 4(C)-(b)) and the weakest point (Fig. 4(C)-(a)) on the GNUs-modified paper substrate. (F) The SERS spectra at the strongest point (Fig. 4(D)-(d)) and the weakest point (Fig. 4(D)-(c)) on the GNUs-modified h-paper substrate. (G) The average SERS spectra of the NBA-labeled GNUs-modified h-paper substrate after the storage of 0 day, 5 days, 10 days, 15 days at room temperature. (H) SERS intensities of the bands at 592 cm^{-1} corresponding to the SERS spectra (G).

Biomedical Optics EXPRESS

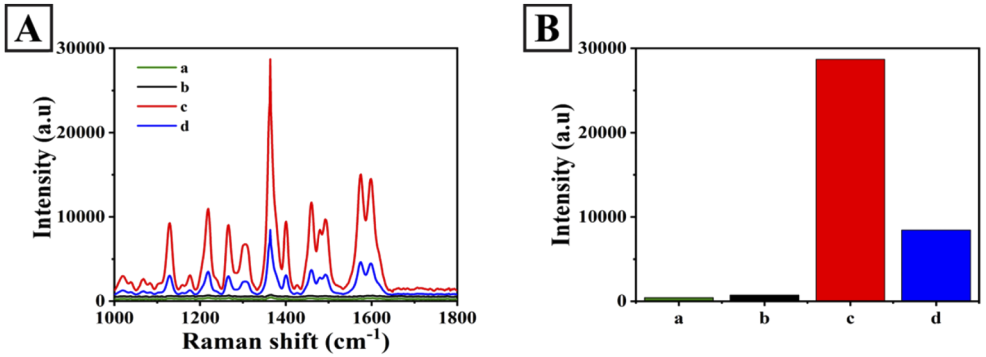

Fig. 5. (A) SERS spectra of the GNUs substrate (curve a), the GNUs substrate with Cyt c aptamer modification (curve b), the GNUs substrate with aptamer and Cy5-labeled complementary DNA (curve c), the SERS biosensor in the presence of Cyt c (curve d). (B) The corresponding intensities bar graphs of characteristic peaks of Cy5 at 1360 cm^{-1}.

3.6. Optimization of experimental conditions

In order to achieve the best performance of the SERS biosensor platform, the experimental conditions were further optimized, including the concentration of Cyt c aptamer, the concentration of Cy5-labeled complementary DNA, hybridization time, incubation time of aptamer bonding to Cyt c and pH values (see Supplement 1, Fig. S2).

3.7. Selectivity and reproducibility of SERS biosensor platform

Under optimal experimental conditions, SERS biosensor platform was constructed to evaluate the selectivity and reproducibility of this approach. To demonstrate the selectivity of the strategy, in addition to Cyt c, five other groups of biologically relevant species including glucose (Glu), immunization globulin G (lgG), human serum albumin (HSA), bovine serum albumin (BSA) and ascorbic acid (AA), at the same concentration of (10 μg/mL) were added to the GNUs substrate and the SERS intensity at 1360 cm^{-1} was measured. From Figs. 6(A) and 6(B), compare with the other control groups, the sample containing Cyt c at the same concentration can efficiently decrease the SERS signal, thus demonstrating that the developed SERS biosensor platform possesses a high selectivity toward the target Cyt c. It can be confirmed from the results that the SERS biosensor platform was capable of tolerating a complex sensing environment. Figures 6(C) and 6(D) showed the reproducibility of SERS biosensor platform. Eight different batches of SERS biosensor platform were prepared at different times. SERS spectra of different batches of SERS biosensor platform for detection of the same sample containing Cyt c (10 μg/mL) were measured. The deviation of peak height at 1360 cm^{-1} was 4.30% (Fig. 6(D)), which supported the good reproducibility of the SERS biosensor platform. The overall results demonstrated excellent selectivity and reproducibility of the SERS biosensor platform toward Cyt c, which can be used as a material for biomarker detection in complex sensing environment.

3.8. Fabricated SERS sensor for Cyt c detection

For quantitative Cyt c detection, eight Cyt c standards were added to the GNUs substrate containing Cyt c aptamer and Cy5-labeled complementary DNA at final Cyt c concentrations of 0 pg/mL, 10 pg/mL, 100 pg/mL, 1 ng/mL, 10 ng/mL, 100 ng/mL, 1 μg/mL and 10 μg/mL in PBS, respectively. As shown in Fig. 7(A), with the concentration of Cyt c increased, SERS intensities of Cy5 characteristic peak gradually decreased. It is due to that the specific binding of Cyt c to its aptamer resulted in the detachment of the complementary chains modified with

Biomedical Optics EXPRESS

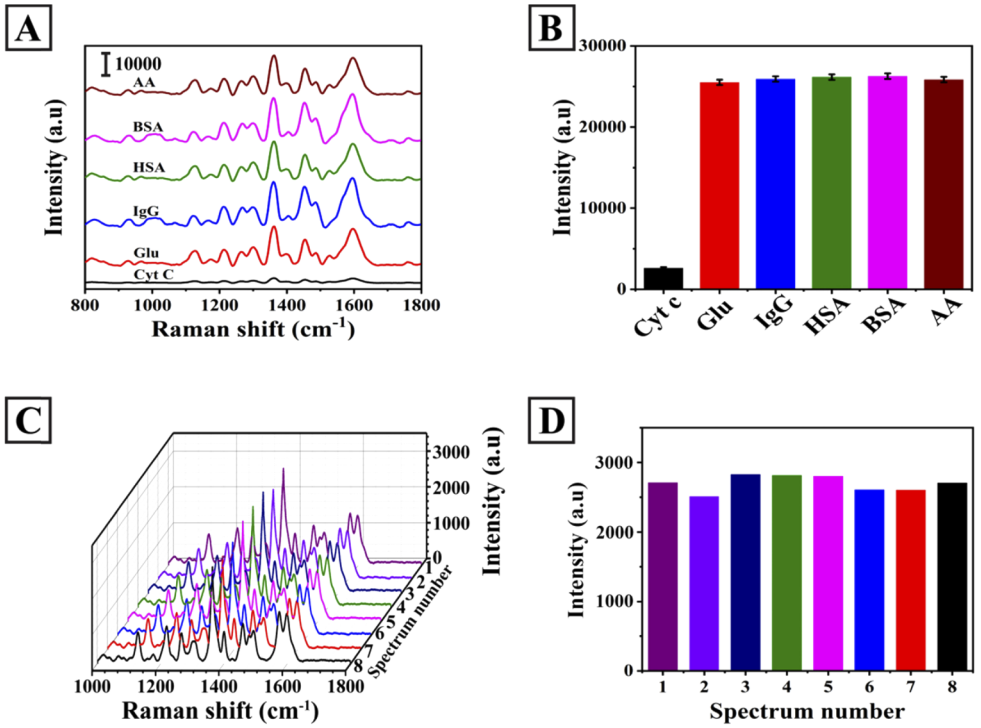

Fig. 6. (A) SERS spectra measured for the detection of Cyt c, glucose (Glu), immunization globulin G (lgG), human serum albumin (HSA), bovine serum albumin (BSA) and ascorbic acid (AA) at the same concentration of 10 μg/mL in PBS. (B) SERS intensities of Cy5 characteristic peak at 1360 cm^{-1} corresponding to A. (C) The reproducibility of SERS biosensor platform. (D) SERS intensities of Cy5 characteristic peak at 1360 cm^{-1} corresponding to C.

Cy5. The characteristic Cy5 peak at 1360 cm^{-1} was chosen to quantitatively analyze Cyt c. Figure 7(B) showed the obtained standard curve for the SERS intensity against the logarithm of the Cyt c concentration over the range of 0 pg/mL to 10 μg/mL. The linear regression equation was y=-3284.1x+25095.4, and the correlation coefficient (R^2) was 0.99177, where y was the peak intensity at 1360 cm^{-1} and x was the log of Cyt c concentrations. The limit of detection (LOD) of Cyt c based on the fabricated SERS biosensor was calculated to be 1.148 pg/mL.

To verify the capability of the fabricated SERS biosensor platform to analyze clinical samples, SERS was applied to quantitatively detect the concentration of Cyt c in the clinical serum. The Cyt c solution was prepared by mixing Cyt c with human serum to obtain concentrations in the range of 0 pg/mL to 10 μg/mL. It was evident that a proportional decrease in the intensity of the band at 1360 cm^{-1} was observed with an increase in the Cyt c concentration (Fig. 7(C)). The Cy5 signal showed a linear increase with the Cyt c concentration in the range of 0 pg/mL to 10 μg/mL. As shown in Fig. 7(D), the regression equation and correlation coefficient were y=-3339.7x+25342.8 and 0.9972, respectively. The lowest detection concentration of the SERS biosensor platform for determination of Cyt c in the human serum was 1.79 pg/mL.

3.9. Accuracy verification of SERS biosensor platform

In order to confirm the practicability of the SERS sensing platform, the collected 60 serum samples were analyzed with our developed sensor. Figure 8(A) showed the mean SERS spectra of different serum samples from healthy people and NSCLC patients. As shown in the corresponding

Biomedical Optics EXPRESS

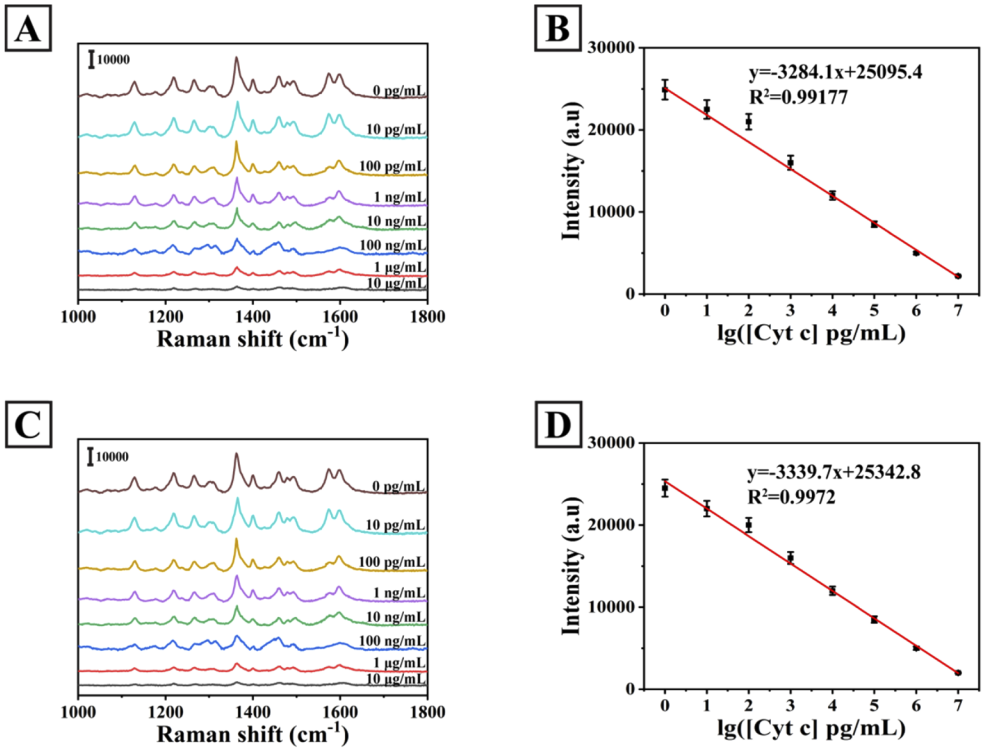

Fig. 7. (A) SERS spectra of Cy5 for quantitative evaluation of the Cyt c with different concentrations from 0 to 10 μg/mL in PBS buffer. (B) Calibration plot of the changed SERS signal intensities (1360 cm^{-1}) versus the logarithm of Cyt c concentrations corresponding to A. (C) SERS spectra of Cy5 for quantitative evaluation of the Cyt c with different concentrations from 0 to 10 μg/mL in the serum. (D) Calibration plot of the changed SERS signal intensities (1360 cm^{-1}) versus the logarithm of Cyt c concentrations corresponding to C.

bar graphs (Fig. 8(B)), the SERS intensities of the peaks at 1360 cm^{-1} of NSCLC patients were much higher than healthy subjects. The concentrations of Cyt c were calculated by substituting the SERS intensities at 1360 cm^{-1} into the linear regression equation obtained in the human serum (Fig. 7(D)). The feasibility of the SERS method for Cyt c quantitative detection was validated using the ELISA method for comparison, and the results were shown in Table 2. The results obtained by the two methods were consistent, which demonstrated the proposed SERS biosensor platform to be a feasible and promising platform for SERS-based quantitative detection of Cyt c in clinical applications.

Table 2. Results of serum samples using SERS and ELISA methods.

Sample	SERS (ng/mL)	ELISA (ng/mL)	Relative error (%)
Healthy subjects	121.2	120.8	0.23
NSCLC	19.3	20.7	-4.95

Biomedical Optics EXPRESS

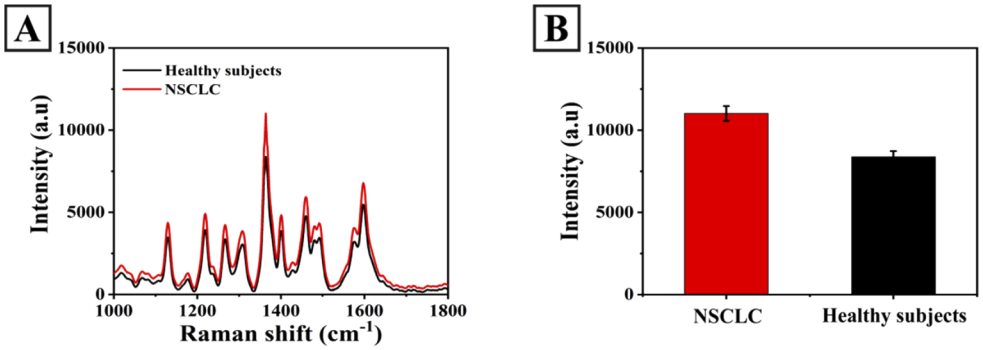

Fig. 8. (A) The mean SERS spectra of different clinical serum samples. (B) The bar charts of the intensities of the peaks at 1360 cm^{-1} corresponding to A.

4. Conclusion

In conclusion, we proposed a simple and sensitive SERS biosensor platform for quantitative detection of Cyt c in the serum of NSCLC patients, which was composed of GNUs-modified h-paper substrate containing Cyt c aptamer and Cy5-labeled complementary DNA. GNUs aggregates had excellent SERS enhancement effect which was confirmed by FDTD simulation. The filter paper was subjected to hydrophobic surface modification by AKD treatment, increasing the density of GNUs decorated on paper. In the further study, by optimizing the reaction conditions, such as the content of Cyt c aptamer and Cy5-labeled complementary DNA, hybridization time, incubation time of Cyt c and pH values, the best performance of the SERS biosensor platform could be achieved. The detection results of Cyt c concentrations in PBS and human serum displayed good linear relationships from 0 pg/mL to 10 μg/mL with detection limit of 1.148 pg/mL and 1.79 pg/mL respectively. In addition, SERS biosensor platform had the advantages of good reproducibility and specificity. Finally, the proposed SERS biosensor platform was successfully used for quantitative detection of Cyt c in clinical serum samples. The low cost and simplicity of this work laid the groundwork for future medical research and clinical treatment of NSCLC.

Funding

National Natural Science Foundation of China (81701825); Social Development Foundation of Jiangsu (BE2018684); Natural Science Research of Jiangsu Higher Education Institutions of China (17KJB416012).

Disclosures

The authors declare that there are no conflicts of interest related to this article.

See Supplement 1 for supporting content.

References

1. D. M. Parkin, F. Bray, J. Ferlay, and P. Pisani, "Global cancer statistics, 2002," Ca-Cancer J. Clin. **55**(2), 74–108 (2005).
2. H. Asamura, T. Goya, Y. Koshiishi, Y. Sohara, K. Eguchi, K. Mori, Y. Nakanishi, R. Tsuchiya, K. Shimokata, H. Inoue, T. Nitkiwa, and E. Miyaoka, "A Japanese lung cancer registry study-Prognosis of 13,010 resected lung cancers," J. Thorac. Oncol. **3**(1), 46–52 (2008).

Biomedical Optics EXPRESS

3. B. Haaland, P. S. Tan, G. J. de Castro, and G. Lopes, "Metaanalysis of first-line therapies in advanced non-small-cell lung cancer harboring EGFR-activating mutations," J. Thorac. Oncol. **9**(6), 805–811 (2014).
4. F. Bray, J. Ferlay, I. Soerjomataram, R. L. Siegel, L. A. Torre, and A. Jemal, "Global cancer statistics 2018: GLOBOCAN estimates of incidence and mortality worldwide for 36 cancers in 185 countries," Ca-Cancer J. Clin. **68**(6), 394–424 (2018).
5. M. Amouzadeh Tabrizi, J. Ferre-Borrull, and L. F. Marsal, "Highly sensitive IRS based biosensor for the determination of cytochrome c as a cancer marker by using nanoporous anodic alumina modified with trypsin," Biosens. Bioelectron. **149**, 111828 (2020).
6. J. B. Li, W. N. Cheng, X. L. Wang, H. J. Zhang, J. Jin, W. Ji, X. X. Han, and B. Zhao, "Electron transfer of cytochrome c on surface-enhanced Raman scattering-active substrates: material dependence and biocompatibility," Chem. - Eur. J. **23**(38), 9034–9038 (2017).
7. J. Y. Zhu, M. W. Jiang, H. Ma, H. J. Zhang, W. N. Cheng, J. B. Li, L. J. Cai, X. X. Han, and B. Zhao, "Redox-state-mediated regulation of cytochrome c release in apoptosis revealed by surface-enhanced Raman scattering on Nickel substrates," Angew. Chem., Int. Ed. **58**(46), 16499–16503 (2019).
8. J. Javid, R. Mir, P. K. Julka, P. C. Ray, and A. Saxena, "Extracellular cytochrome c as a biomarker for monitoring therapeutic efficacy and prognosis of non-small cell lung cancer patients," Tumor Biol. **36**(6), 4253–4260 (2015).
9. L. Yang and J. H. Yang, "Expression and clinical significance of microRNA-21, PTEN and p27 in cancer tissues of patients with non-small cell lung cancer," Oncol. Lett. **20**(4), 1 (2020).
10. L. Yang, M. X. Gao, L. Zhan, M. Gong, S. J. Zhen, and C. Z. Huang, "An enzyme-induced Au@Ag core-shell nanoStructure used for an ultrasensitive surface-enhanced Raman scattering immunoassay of cancer biomarkers," Nanoscale **9**(7), 2640–2645 (2017).
11. Y. D. Sun, L. Shi, L. Mi, R. Y. Guo, and T. Li, "Recent progress of SERS optical nanosensors for miRNA analysis," J. Mater. Chem. B **8**(24), 5178–5183 (2020).
12. K. C. Bantz, A. F. Meyer, N. J. Wittenberg, H. Im, O. Kurtuluş, S. H. Lee, N. C. Lindquist, S. H. Oh, and C. L. Haynes, "Recent progress in SERS biosensing," Phys. Chem. Chem. Phys. **13**(24), 11551–11567 (2011).
13. C. Zhang, S. Z. Jiang, Y. Y. Huo, A. H. Liu, S. C. Xu, X. Y. Liu, Z. C. Sun, Y. Y. Xu, Z. Li, and B. Y. Man, "SERS detection of R6G based on a novel graphene oxide/silver nanoparticles/silicon pyramid arrays structure," Opt. Express **23**(19), 24811–24821 (2015).
14. P. Guo, D. Sikdar, X. Huang, K. J. Si, W. Xiong, S. Gong, L. W. Yap, M. Premaratne, and W. Cheng, "Plasmonic core-shell nanoparticles for SERS detection of the pesticide thiram: size- and shape-dependent Raman enhancement," Nanoscale **7**(7), 2862–2868 (2015).
15. S. Li, L. Xu, W. Ma, H. Kuang, L. Wang, and C. Xu, "Triple Raman label-encoded gold nanoparticle trimers for simultaneous heavy metal ion detection," Small **11**(28), 3435–3439 (2015).
16. R. Zhang, Y. Zhang, Z. C. Dong, S. Jiang, C. Zhang, L. G. Chen, L. Zhang, Y. Liao, J. Aizpurua, Y. Luo, J. L. Yang, and J. G. Hou, "Chemical mapping of a single molecule by plasmon-enhanced Raman scattering," Nature **498**(7452), 82–86 (2013).
17. R. A. Alvarez-Puebla and L. M. Liz-Marzan, "SERS-based diagnosis and biodetection," Small **6**(5), 604–610 (2010).
18. X. Lu, Y. Huang, B. Liu, L. Zhang, L. Song, J. Zhang, A. Zhang, and T. Chen, "Light-controlled shrinkage of large-area gold nanoparticle monolayer film for tunable SERS activity," Chem. Mater. **30**(6), 1989–1997 (2018).
19. B. X. Hu, D. W. Sun, H. B. Pu, and Q. Y. Wen, "Rapid nondestructive detection of mixed pesticides residues on fruit surface using SERS combined with self-modeling mixture analysis method," Talanta **217**, 120998 (2020).
20. M. Bhamidipati and L. Fabris, "Multiparametric assessment of gold nanoparticle cytotoxicity in cancerous and healthy cells: the role of size, shape, and surface chemistry," Bioconjugate Chem. **28**(2), 449–460 (2017).
21. C. Zhang, C. H. Li, J. Yu, S. Z. Jiang, S. C. Xu, C. Yang, Y. J. Liu, X. G. Gao, A. H. Liu, and B. Y. Man, "SERS activated platform with three-dimensional hot spots and tunable nanometer gap," Sens. Actuators, B **258**, 163–171 (2018).
22. V. Tran, C. Thiel, J. T. Svejda, M. Jalali, B. Walkenfort, D. Erni, and S. Schlucker, "Probing the SERS brightness of individual Au nanoparticles, hollow Au/Ag nanoshells, Au nanostars and Au core/Au satellite particles: single-particle experiments and computer simulations," Nanoscale **10**(46), 21721–21731 (2018).
23. R. E. Ionescu, E. N. Aybeke, E. Bourillot, Y. Lacroute, E. Lesniewska, P. M. Adam, and J. L. Bijeon, "Fabrication of annealed gold nanostructures on pre-treated glow-discharge cleaned glasses and their used for localized surface plasmon resonance (LSPR) and surface enhanced Raman spectroscopy (SERS) detection of adsorbed (bio)molecules," Sensors **17**(2), 236–246 (2017).
24. M. J. Schnepf, M. Mayer, C. Kuttner, M. Tebbe, D. Wolf, M. Dulle, T. Altantzis, P. Formanek, S. Foerster, S. Bals, T. A. F. Koenig, and A. Fery, "Nanorattles with tailored electric field enhancement," Nanoscale **9**(27), 9376–9385 (2017).
25. S. D. Jayasena, "Aptamers: an emerging class of molecules that rival antibodies in diagnostics," Clin. Chem. **45**(9), 1628–1650 (1999).
26. Z. Hao, Z. R. Wang, Y. J. Li, Y. B. Zhu, X. J. Wang, C. G. De Moraes, Y. L. Pan, X. Z. Zhao, and Q. Lin, "Measurement of cytokine biomarkers using an aptamer-based affinity graphene nanosensor on a flexible substrate toward wearable applications," Nanoscale **10**(46), 21681–21688 (2018).
27. H. D. Wang, X. W. Huang, G. Q. Wen, and Z. L. Jiang, "A dual-model SERS and RRS analytical platform for Pb(II) based on Ag-doped carbon dot catalytic amplification and aptamer regulation," Sci. Rep. **9**(1), 9991 (2019).

Biomedical Optics EXPRESS

28. M. Bhamidipati, H. Y. Cho, K. B. Lee, and L. Fabris, "SERS-based quantification of biomarker expression at the single cell level enabled by gold nanostars and truncated aptamers," Bioconjugate Chem. **29**(9), 2970–2981 (2018).
29. J. H. Lee, M. V. Yigit, D. Mazumdar, and Y. Lu, "Molecular diagnostic and drug delivery agents based on aptamer-nanomaterial conjugates," Adv. Drug Delivery Rev. **62**(6), 592–605 (2010).
30. X. Pang, C. Cui, S. Wan, Y. Jiang, L. Zhang, L. Xia, L. Li, X. Li, and W. Tan, "Bioapplications of cell-SELEX-generated aptamers in cancer diagnostics, therapeutics, theranostics and biomarker discovery: a comprehensive review," Cancers **10**(2), 47 (2018).
31. D. Shangguan, L. Meng, Z. C. Cao, Z. Xiao, X. Fang, Y. Li, D. Cardona, R. P. Witek, C. Liu, and W. Tan, "Identification of liver cancer-specific aptamers using whole live cells," Anal. Chem. **80**(3), 721–728 (2008).
32. S. Yoon and J. J. Rossi, "Targeted molecular imaging using aptamers in cancer," Pharmaceuticals **11**(3), 71–87 (2018).
33. Q. Wang, Y. J. Hu, N. J. Jiang, J. J. Wang, M. Yu, and X. M. Zhuang, "Preparation of aptamer responsive DNA functionalized hydrogels for the sensitive detection of α-fetoprotein using SERS method," Bioconjugate Chem. **31**(3), 813–820 (2020).
34. Y. Y. Li, Q. Q. Fang, X. X. Miao, X. Y. Zhang, Y. Zhao, J. Yan, Y. Q. Zhang, R. F. Wu, B. Q. Nie, M. Hirtz, and J. Liu, "Aptamer conformation-cooperated enzyme-assisted surface-enhanced Raman scattering enabling ultrasensitive detection of cell surface protein biomarkers in blood samples," ACS Sens. **4**(10), 2605–2614 (2019).
35. L. A. Lane, X. M. Qian, and S. M. Nie, "SERS nanoparticles in medicine: from label-free detection to spectroscopic tagging," Chem. Rev. **115**(19), 10489–10529 (2015).
36. S. Y. Ding, E. M. You, Z. Q. Tian, and M. Moskovits, "Electromagnetic theories of surface-enhanced Raman spectroscopy," Chem. Soc. Rev. **46**(13), 4042–4076 (2017).
37. M. Mohammadpour, M. H. Khodabandeh, L. Visscher, and Z. Jamshidi, "Elucidation of charge-transfer SERS selection rules by considering the excited state properties and the role of electrode potential," Phys. Chem. Chem. Phys. **19**(11), 7833–7843 (2017).
38. J. Feng, Y. J. Xu, W. Y. Huang, H. X. Kong, Y. Q. Li, H. Cheng, and L. J. Li, "A magnetic SERS immunosensor for highly sensitive and selective detection of human carboxylesterase 1 in human serum samples," Anal. Chim. Acta **1097**, 176–185 (2020).
39. C. L. Zhao, L. H. Qiu, P. Lv, A. L. Han, G. Z. Fang, J. F. Liu, and S. Wang, "AuNP-peptide probe for caspase-3 detection in living cells by SERS," Analyst **144**(4), 1275–1281 (2019).
40. Y. T. Long, H. Li, Z. J. Du, M. M. Geng, and Z. R. Liu, "Confined Gaussian-distributed electromagnetic field of tin(II) chloride-sensitized surface-enhanced Raman scattering (SERS) optical fiber probe: From localized surface plasmon resonance (LSPR) to waveguide propagation," J. Colloid Interface Sci. **581**, 698–708 (2021).
41. L. Q. Tan, C. Liu, Y. Wang, J. Sun, J. Dong, and W. P. Qian, "Fabrication of SERS substrates containing dense "hot spots" by assembling star-shaped nanoparticles on superhydrophobic surfaces," New J. Chem. **41**(12), 5028–5033 (2017).
42. M. Muhammad, C. S. Shao, and Q. Huang, "Label-free SERS diagnostics of radiation-induced injury via detecting the biomarker Raman signal in the serum and urine bio-samples based on Au-NPs array substrates," Spectrochim. Acta, Part A **223**, 117282 (2019).
43. X. Zhou, G. Q. Liu, H. W. Zhang, Y. Li, and W. P. Cai, "Porous zeolite imidazole framework-wrapped urchin-like Au-Ag nanocrystals for SERS detection of trace hexachlorocyclohexane pesticides via efficient enrichment," J. Hazard. Mater. **368**, 429–435 (2019).
44. Y. F. Tian, W. Zhou, B. C. Yin, and B. C. Ye, "Highly sensitive surface-enhanced Raman scattering detection of adenosine triphosphate based on core-satellite assemblies," Anal. Methods **9**(42), 6038–6043 (2017).
45. R. Purbia, P. D. Nayak, and S. Paria, "Visible light-induced Ag nanoparticle deposited urchin-like structures for enhanced SERS application," Nanoscale **10**(27), 12970–12974 (2018).
46. H. Y. Chen, M. H. Lin, C. Y. Wang, Y. M. Chang, and S. Gwo, "Large-scale hot spot engineering for quantitative SERS at the single-molecule scale," J. Am. Chem. Soc. **137**(42), 13698–13705 (2015).
47. M. Lee, K. Oh, H. K. Choi, S. G. Lee, H. J. Youn, H. L. Lee, and D. H. Jeong, "Subnanomolar sensitivity of filter paper-based SERS sensor for pesticide detection by hydrophobicity change of paper surface," ACS Sens. **3**(1), 151–159 (2018).
48. D. J. Lee and D. Y. Kim, "Hydrophobic paper-based SERS sensor using gold nanoparticles arranged on graphene oxide flakes," Sensors **19**(24), 5471–5480 (2019).
49. C. Q. Han, Y. Q. Li, Q. Jia, L. H. Bradley, Y. Gan, Y. Yao, L. L. Qu, H. T. Li, and Y. P. Zhao, "On-demand fabrication of surface-enhanced Raman scattering arrays by pen writing, and their application to the determination of melamine in milk," Microchim. Acta **184**(8), 2909–2917 (2017).
50. Y. Guo, J. Yu, C. H. Li, Z. Li, J. Pan, A. H. Liu, B. Y. Man, T. F. Wu, X. W. Xiu, and C. Zhang, "SERS substrate based on the flexible hybrid of polydimethylsiloxane and silver colloid decorated with silver nanoparticles," Opt. Express **26**(17), 21784–21796 (2018).
51. J. N. Zhang, X. Y. Ma, and Z. P. Wang, "Surface-enhanced Raman scattering-fluorescence dual-mode nanosensors for quantitative detection of cytochrome c in living cells," Anal. Chem. **91**(10), 6600–6607 (2019).
52. U. Hundhausen, H. Militz, and C. Mai, "Use of alkyl ketene dimer (AKD) for surface modification of particleboard chips," Eur. J. Wood Wood Prod. **67**(1), 37–45 (2009).

Biomedical Optics EXPRESS

53. W. G. Qu, S. M. Wang, Z. J. Hu, T. Y. Cheang, Z. H. Xing, X. J. Zhang, and A. W. Xu, "In situ synthesis of gold@3,4-dihydroxy-L-phenylalanine core-shell nanospheres used for cell imaging," J. Phys. Chem. C **114**(30), 13010–13016 (2010).
54. Z. Liu, F. L. Zhang, Z. B. Yang, H. J. You, C. F. Tian, Z. Y. Lib, and J. X. Fang, "Gold mesoparticles with precisely controlled surface topographies for single-particle surface-enhanced Raman spectroscopy," J. Mater. Chem. C **1**(35), 5567–5576 (2013).
55. J. H. Xu, C. H. Li, H. P. Si, X. F. Zhao, L. Wang, S. Z. Jiang, D. M. Wei, J. Yu, X. W. Xiu, and C. Zhang, "3D SERS substrate based on Au-Ag bi-metal nanoparticles/MoS hybrid with pyramid structure," Opt. Express **26**(17), 21546–21557 (2018).
56. Z. Li, S. Z. Jiang, Y. Y. Huo, T. Y. Ning, A. H. Liu, C. Zhang, Y. He, M. H. Wang, C. H. Li, and B. Y. Man, "3D silver nanoparticles with multilayer graphene oxide as a spacer for surface enhanced Raman spectroscopy analysis," Nanoscale **10**(13), 5897–5905 (2018).
57. Y. Wu, F. B. Xiao, Z. Y. Wu, and R. Q. Yu, "Novel aptasensor platform based on ratiometric surface-enhanced Raman spectroscopy," Anal. Chem. **89**(5), 2852–2858 (2017).